IEEE Photonics Journal
An IEEE Photonics Society Publication

Open Access

Electrically Controllable Liquid Crystal Component for Efficient Light Steering

Volume 7, Number 2, April 2015

Xiaobing Shang
Jin-Yi Tan
Oliver Willekens
Jelle De Smet
Pankaj Joshi
Dieter Cuypers
Esma Islamaj
Jeroen Beeckman
Kristiaan Neyts
Michael Vervaeke
Hugo Thienpont
Herbert De Smet

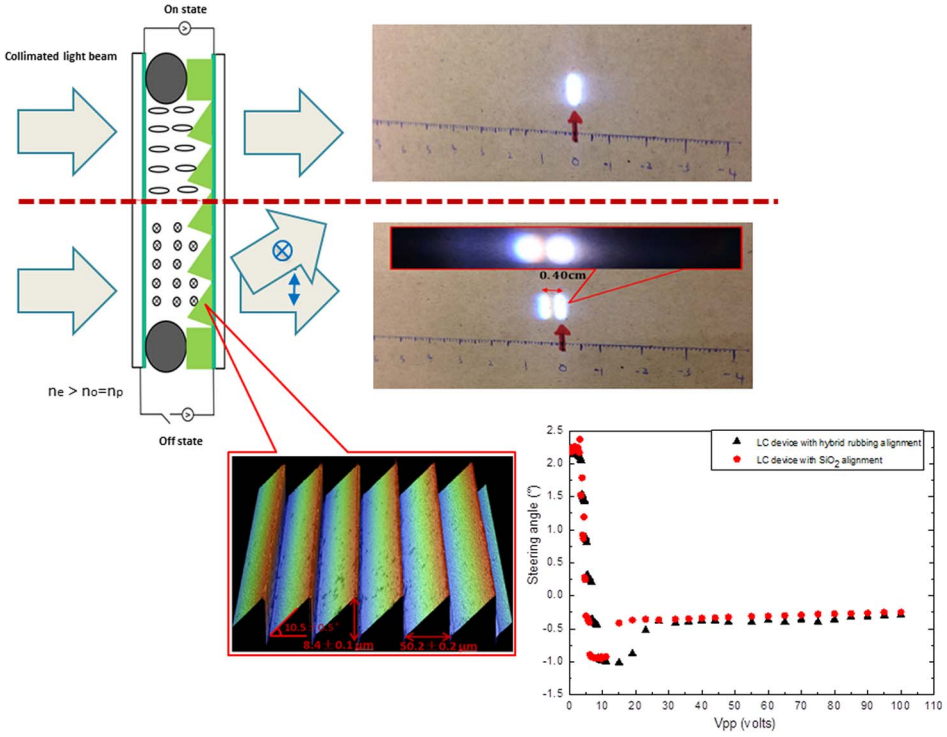

Electrically tunable beam steering components with the combination of micro-prism and liquid crystals.

DOI: 10.1109/JPHOT.2015.2402592

Electrically Controllable Liquid Crystal Component for Efficient Light Steering

Xiaobing Shang,[1] Jin-Yi Tan,[1] Oliver Willekens,[2] Jelle De Smet,[1] Pankaj Joshi,[1] Dieter Cuypers,[1] Esma Islamaj,[1] Jeroen Beeckman,[2] Kristiaan Neyts,[2] Michael Vervaeke,[3] Hugo Thienpont,[3] and Herbert De Smet[1]

[1]Centre for Microsystems Technology, Ghent University and IMEC, 9052 Ghent, Belgium
[2]Liquid Crystal and Photonics Group, Ghent University, 9000 Ghent, Belgium
[3]Brussels Photonics Team, Vrije Universiteit Brussel, 1050 Brussels, Belgium

DOI: 10.1109/JPHOT.2015.2402592

Manuscript received January 14, 2015; revised February 5, 2015; accepted February 7, 2015. Date of publication February 11, 2015; date of current version February 25, 2015. This work was supported by the IWT through the SBO project SECONDOS, IWT-nr 120019, 2013–2016. Corresponding author: X. Shang (e-mail: xiaobing_shang@hotmail.com).

Abstract: In this paper, we present an electrically controllable microoptical component for light beam steering and light intensity distribution built on the combination of nematic liquid crystal (LC) and polymer microprisms. Polymer microprism arrays are fabricated using soft embossing with elastic polydimethylsiloxane molds and ultraviolet curable resins. Surface profiling measurements show that the dimensions of the replicated prisms closely approximate those of the master prism. Two different LC alignment techniques were employed: hybrid rubbing alignment and obliquely evaporated SiO_2 alignment, both of which result in proper alignment of the LC molecules along the prism groove direction. The operation voltage of the LC components is relatively low (10 V_{rms}). The steering angle of a green laser beam was experimentally studied as a function of applied voltage, and a steering range of 3° was found. The active LC components also effectively deflect a collimated white light beam over a steering angle of about 2° with an efficiency of 27%–33%. All the optical measurements are in agreement with theoretical calculations based on Snell's law.

Index Terms: Beam steering, light intensity distribution, transmissive microprism, liquid crystal prism, liquid crystal alignment, soft embossing.

1. Introduction

Dynamic manipulation of light beams is of vital importance to many optical and photonic applications (stage lightings, autostereoscopic displays, and laser scanners). Using a mechanical approach based on mirrors, prisms and lenses usually leads to a costly and too bulky system which does not have the desired flexibility and reliability [1]–[3]. Beam steering devices based on the micro-electro-mechanical systems (MEMS) rely on the decentered micro lens technique, the positional or angular displacements of the curved or other specially designed micro mirrors to deflect the incident light beam, allowing the development of many innovative photonic products [4]–[6], but their major limitations are the intricate device structures, complicated fabrication processes, and very small working dimensions. It is well known that nematic liquid crystal (NLC) is a material with interesting optical and electrical properties. It consists of oblong molecules that tend to align parallel to each other but otherwise can freely move as molecules in a liquid.

From an optical point of view, NLC is birefringent, i.e., it exhibits a different refractive index for the ordinary rays (rays with their electrical field vector perpendicular to the molecular axis) than for the extraordinary rays (electrical field vector parallel to the molecular axis) [7]. Due to the dielectric effect the LC molecules experience the influence of an applied electrical field, and reorient themselves if the field is stronger than a certain threshold value [8]. As a result, the effective refractive index of the material is electrically tunable for the incoming light, making liquid crystal a good material for dynamic optical components and imaging devices. Beam steering devices based on the gradient refractive index (GRIN) effect have attracted intensive interest; most of them are based on nonuniform electric field, inhomogeneously distributed polymer networks or special surface alignment to induce the gradient refractive index inside the LC layers in order to realize the beam steering [9]–[13]. These devices either need complex driving circuits or sophisticated and unmanageable fabricating techniques. Moreover, the nonuniform LC orientations within these devices easily result in serious disclinations and defects occurring in the LC textures which largely degrade the beam steering property [14]. To overcome the above drawbacks, the combination of the micro prism with NLC was investigated in this work. This kind of device not only enables the continuous electrical tunability that conventional optical components (prisms, lenses and gratings) cannot offer, but also its fabrication process is simpler and easily controllable compared to the MEMS devices and the GRIN-LC components. It is also compatible with the currently dominant LC display technology and the micro-imprinting lithography, tunable beam steering devices with large working areas based on this technology are accessible for the lighting industry and large autostereoscopic displays and so forth.

Since Chou *et al.* proposed the nano imprint lithography technique [15], this technology has been broadly used for various kinds of surface patterning. Especially imprinting with negative polydimethylsiloxane (PDMS) molds and ultraviolet (UV) curable materials, soft embossing has emerged as a novel technology for polymer micro-structures fabrication [16]–[18]. Compared with other micro-structure fabrication technologies including the injection molding [19], diamond tooling [20], hot embossing [21], and laser processing [22], soft embossing is simple and highly efficient. It neither requires high temperatures nor a heavy press, leading to large areas of micro-optical structures without birefringence or thermal damage. Because of the enormous choice of available UV resins [23], it is almost always possible to find one with optimized properties for the optical component fabrications one is envisaging [24]. Moreover, soft embossing combined with a roll to roll process could prove to be a better way for low-cost mass production of micro-optical products [25], [26]. In the study, soft embossing with PDMS molds and UV curable resins is employed in the fabrication of micro-prism structures on ITO glass substrates for the build-up of LC beam steering components.

The electro-optical properties of LC devices are largely dependent on the liquid crystal alignment. For example, a weak LC alignment is known to reduce the operating voltage and increase the response time [27], [28]. In the past decades, several LC alignment techniques were developed to induce uniform liquid crystal orientations [29]. Since the rubbed polyimide method requires a high temperature for curing the polyimide, above the melting point of the UV prism, it is very challenging to apply the polyimide layer to the prism directly. In this work we have investigated if directly rubbing along the prism grooves could also result in anchoring of the LC molecules along the desired direction. The second available technique is oblique SiO_2 evaporation on the prism surface, which is a process that takes place at low temperatures. Electrically controllable LC beam steering components based on these two LC alignment techniques were fabricated, fully characterized, and analyzed.

2. Experimental

2.1. Fabrication of Micro Prism Structures by Soft Embossing

The soft embossing process in our experiments mainly consists of two steps. The first step is the fabrication of elastic PDMS mold based on a master prism, as is shown in Fig. 1(a). The

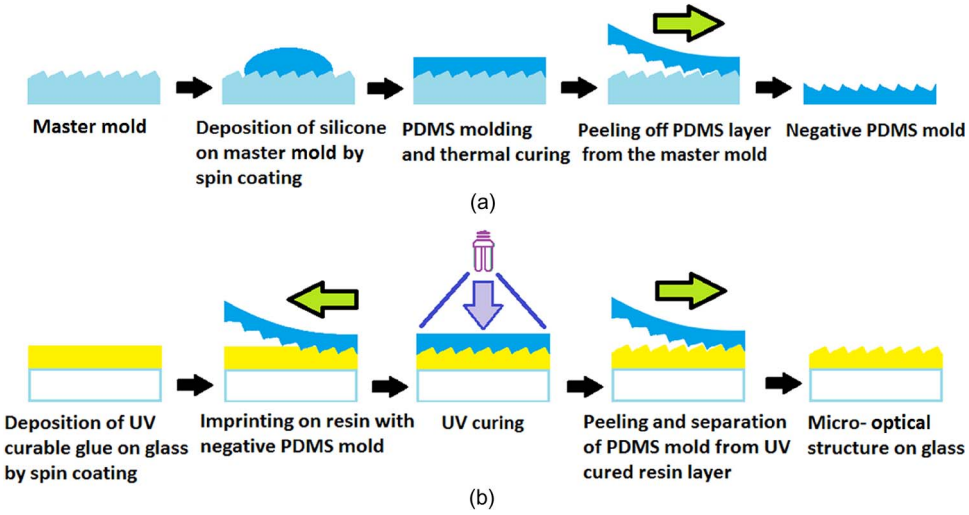

Fig. 1. Schematic flow of the soft embossing process. (a) Elastic PDMS mold fabrication. (b) Imprinting of micro-optical prism structures in the UV glue layer.

TABLE 1

Physical and optical properties of UV curable resins

Name	Viscosity at 25 °C (cps)	Refractive index at 589 nm	Transmission (400 nm−750 nm)
NOA 73	130	1.56	$> 98\%$
NOA 74	80−95	1.52	$> 98\%$
NOA 89	15−20	1.51	$> 98\%$

master prism was hot embossed on the 0.5 mm thick PMMA sheets by B-phot with the Jenoptik HEX04 equipment. A Sylgard 184 (Dow Corning) silicone base is mixed with a curing agent by the ratio of 10 : 1, and degased. Then, the liquid silicone is spin coated (maximum spinning speed of 200 rpm with acceleration of 50 rpm/s, 35s) on top of the PMMA prisms sheet, and cured at 70 °C for 1 hour. The resulting negative PDMS mold is peeled off along the prism groove direction to avoid damage.

The viscosity of the UV glue is a parameter of vital importance. Very low values will make the replication process more difficult as the glue will get expelled during the PDMS mold lamination. Higher values will preclude the glue from following the sharp aspects of the mold morphology, resulting in imperfect prism structures. In our experiments, three UV curable optical resins with different physical properties are used, as shown in Table 1 [24]. In order to satisfy the glue thickness requirement for replication, different spinning speeds (NOA 73: 1000 rpm, NOA 74: 800 rpm and NOA 89: 500 rpm) are adopted to get sufficient glue thickness (NOA 73: 15.3 ± 0.2 μm, NOA 74: 14.7 ± 0.2 μm, and NOA 89: 13.4 ± 0.2 μm). With the above PDMS mold (51×51 mm wide, 1 mm thick), micro-prism structures are replicated onto NOA 73 and NOA 74 using the process shown in Fig. 1(b). The glue is cured during 5 minutes using an incoming UV irradiance of 60 mW/cm^2 and $\lambda = 365$ nm that traverses the PDMS mold. Next, the PDMS mold is peeled off along the prism grooves. The resulting replicated UV prisms are post cured with the same UV irradiance for another 5 minutes. In this experiment, we have observed that for the glue type NOA 89, insufficient glue is present in the area covered by the PDMS mold and as a consequence, no structures are formed. This is explained by the fact that NOA 89, which has the lowest viscosity among the three glues, gets expelled during the PDMS lamination, and too little glue remains in that area for successful PDMS replication.

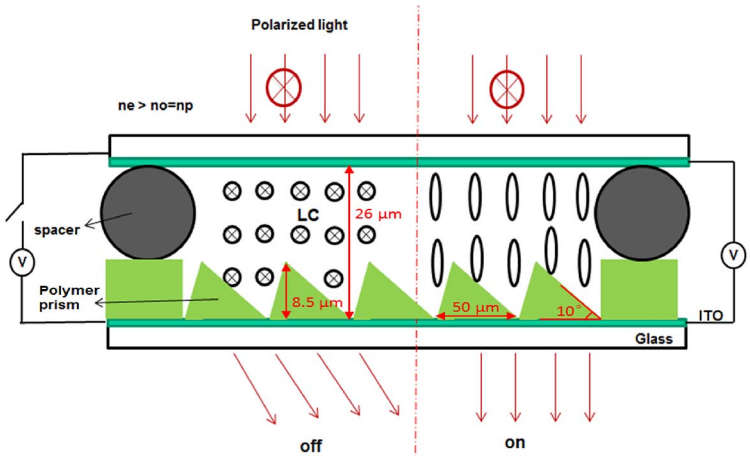

Fig. 2. Cross-section of the proposed active LC beam steering component.

2.2. Fabrication of Liquid Crystal Beam Steering Component

In this part, we combine liquid crystal with the above micro prisms. Since the refractive index of NOA 74 resin equals that of the ordinary ray of nematic LC E7 ($n_o = 1.5224$, $n_e = 1.7394$ with $\lambda = 589$ nm), micro prisms based on NOA 74 are fabricated on the top of one ITO (indium tin oxide) glass substrate by the aforementioned soft embossing process. For the rubbing alignment technique, the nylon solution is spin coated on the ITO glass and cured at 180 °C for 4 hours, since the maximum temperature that the UV prisms can withstand is 90 °C, it is quite challenging to apply the nylon layer onto the prism surface. However, it is thought that the tiny grooves of the prisms could play a role in aligning the LC molecules, and direct rubbing on the prisms along the groove direction is likely to further enhance the anchoring effect. Both cases (with and without rubbing along the prism) will be studied in our experiments. Another LC alignment method available in our lab is oblique evaporation of SiO_2 at low temperature on top of the micro-prism. In this technique, the micro-prism is mounted onto a holder which is oriented at 45° with respect to the evaporation direction, resulting in an angle of 35° between the shallow slope of the prism and the direction of the evaporated SiO_2 beam. With the alignment layers well introduced on the prism and ITO counter glass surface, the two substrates are then assembled together to form a cell. First, UV-curable glue mixed with spacers is applied on the surrounding area of the prism to produce a gasket with an entrance for subsequent LC filling. Then the top and bottom substrates are bonded together with the ITO of the top substrate facing the micro prism of the bottom substrate, forming an anti-parallel LC alignment within the cell. Next, the assembly is placed in a press machine with certain pressure to hold and press the substrates together, while UV light ($I = 50$ mW and $\lambda = 365$ nm) is simultaneously irradiating the cell for 2 minutes to cure the glue border. Finally, the empty cell is filled with nematic LC E7 using vacuum filling. The resulting active LC component with the designed dimensions is schematically illustrated in Fig. 2.

Three different surface treatments for LC alignment are used to the prism substrates: bare prism, bare prism with direct rubbing along the grooves and prism coated with an obliquely evaporated SiO_2 layer. The former two prism substrates are assembled with ITO coated counter glass substrates onto which rubbed nylon alignment layers have been applied, forming anti-parallel LC orientations along the prism groove direction (listed as “single sided nylon alignment” and “hybrid rubbing alignment”, respectively). The third prism, which is coated with the SiO_2 layer, is combined with a flat ITO glass that is also coated with an obliquely evaporated SiO_2 layer to form anti-parallel LC alignment along the prism grooves (listed as “SiO_2 alignment”).

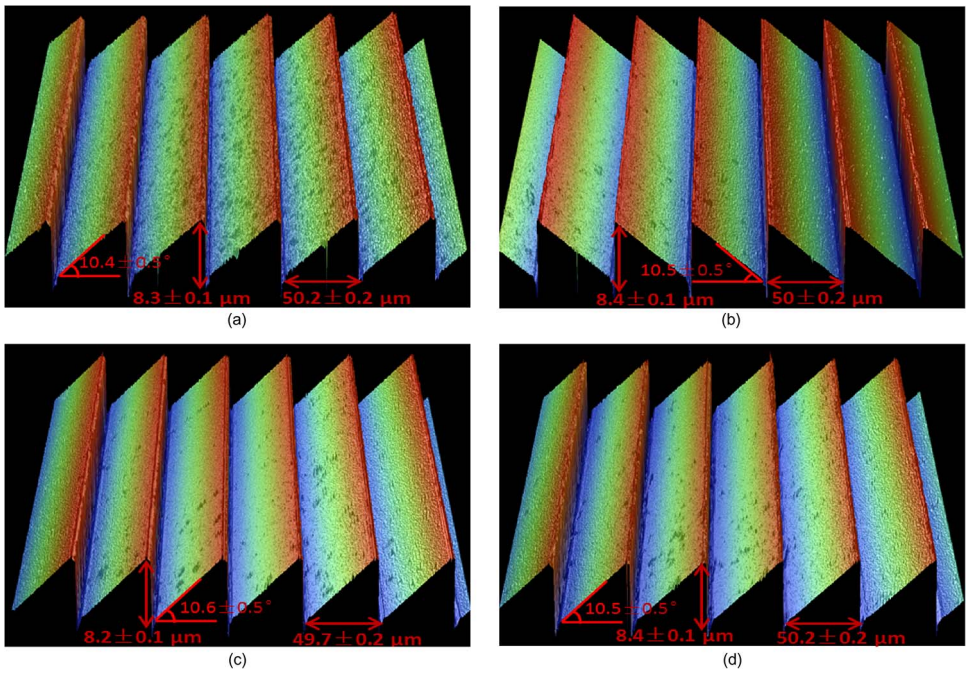

Fig. 3. Surface profile characterization by WYKO. (a) Master prism on PMMA sheet. (b) Replicated PDMS mold. (c) NOA 73 replica. (d) NOA 74 replica.

3. Characterization

3.1. Profile of Micro Prism Structures

The PMMA master prism, negative PDMS mold, and replicated UV prisms with NOA 73 and NOA 74 are characterized using a surface profiler (WYKO NT3300), and the relevant dimensions are indicated in Fig. 3. The pitch, height, and blaze angle of the negative PDMS mold are very close to those of the master prism. Moreover, the dimensions of NOA 73 and NOA 74 replicated from the PDMS mold also approximate those of the master prism. From the prism tip to the flat surrounding surface, the distance is about 7.5 μm, the total LC layer from the top ITO surface to the bottom prism valley for single sided nylon alignment and hybrid rubbing alignment is about 24 μm in thickness and 26 μm for SiO_2 alignment.

The surface roughness of the PMMA master prism, the PDMS mold and the replicated UV prisms are also obtained from the profile measurements, depicted in Fig. 4. It is seen that both the average roughness and root mean square roughness of the negative PDMS mold are a factor two lower than those of the master prism, and the replicated UV prisms (NOA 73 and NOA 74) have a similar roughness as the PDMS mold. This is because the silicone has an extremely high viscosity (3500 cps) compared with those of the UV glues. It is known that high viscosity plays a negative role in the process of liquid filling into the tiny apertures [16]. In addition, after the spin coating of the silicone, the samples are immediately baked at 70 °C for 1 hour. During that step, the viscosity of the silicones increases, which further prevents the silicone from filling the tiny sags and crests that constitute the poor surface roughness. As a result, the roughness of the PDMS mold is better than that of the master prism. The UV curable resins have viscosities that are much lower than that of the silicone, and therefore, these liquid glues easily fill the micro structures and tiny apertures of defects. As a result, they have a similar surface roughness as the PDMS mold.

The above measurements indicate that the replication from the master prism by soft embossing is very successful. Moreover, the availability of a wide range of UV glues with different refractive indices makes the soft embossing process very versatile in the sense that for many different LC materials a matching glue can be found to fabricate beam steering components.

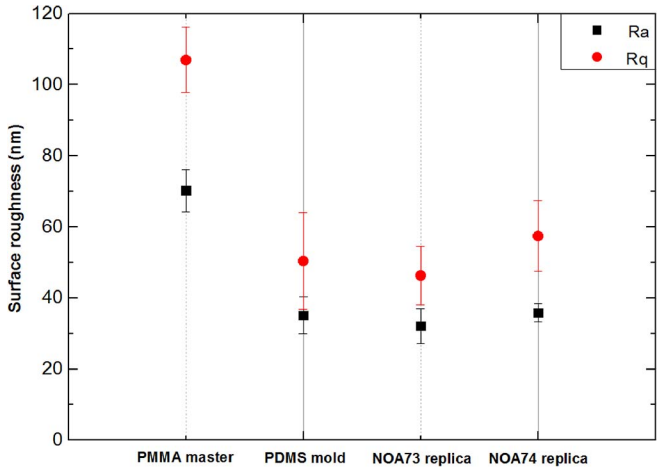

Fig. 4. Surface roughness Ra and Rq of PMMA master prism, negative PDMS mold, NOA 73 replica, and NOA 74 replica. Ra = average roughness (black squares). Rq = root mean square roughness (red circles).

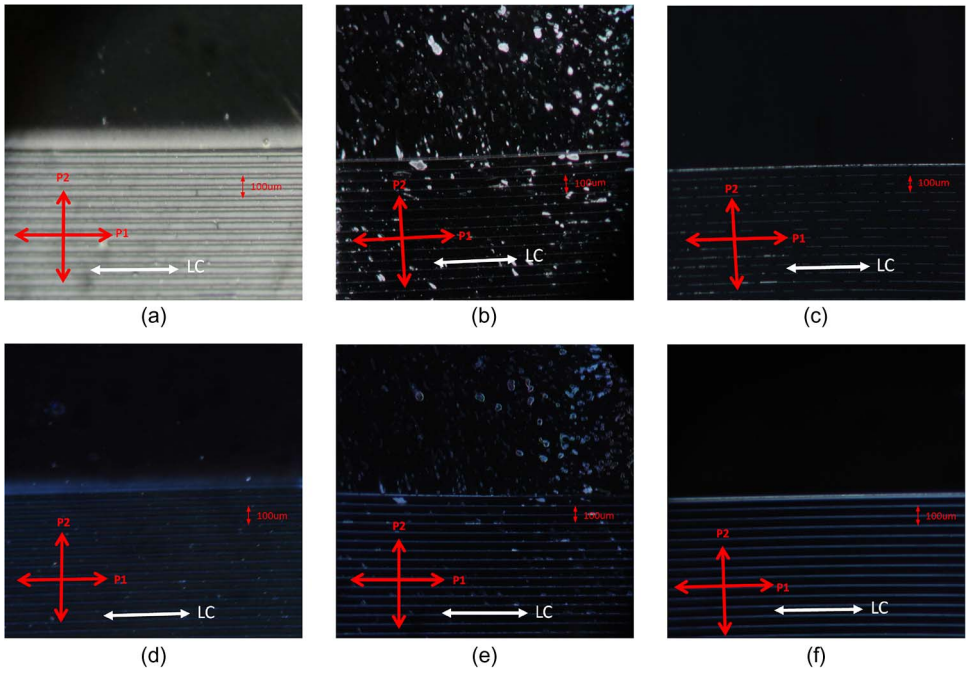

Fig. 5. Liquid crystal alignment of the three schemes under the crossed polarizer microscope. Without electric field. (a) Single sided nylon alignment. (b) Hybrid rubbing alignment. (c) SiO_2 alignment. With applied voltage of 100 V_{pp}. (d) Single sided nylon alignment. (e) Hybrid rubbing alignment. (f) SiO_2 alignment.

3.2. Liquid Crystal Alignment in Active Beam Steering Components

To verify the LC alignment in the active components based on the three schemes mentioned in Section 2.2, the samples are characterized using a crossed polarizer microscope, and the results are shown in Fig. 5. The two crossed red double arrows indicate the transmission axes of the polarizer (P1) and analyzer (P2); the white one represents the expected direction of the liquid crystal alignment.

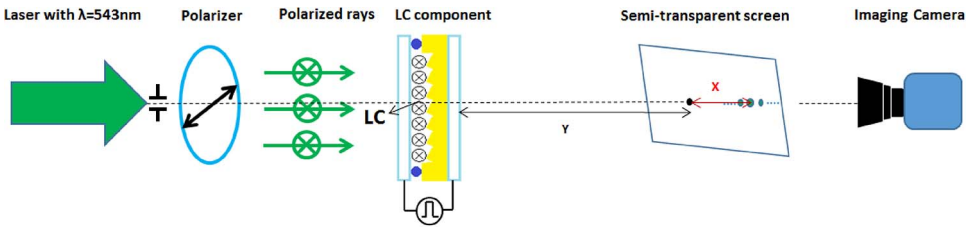

Fig. 6. Schematic setup for optical measurement of liquid crystal beam steering components.

Fig. 5(a)–(c), respectively, show the LC alignment in the three schemes without applying an electric field. With the liquid crystal well aligned parallel to the bottom polarizer (P1), the resultant image should be completely dark, since there is no birefringence and the linear polarization of the incident beam remains constant all the time. Fig. 5(a) demonstrates that the prism area is very bright in single sided nylon alignment, which implies that the prism grooves themselves do not exert any significant alignment effect on the LC molecules. Hybrid rubbing alignment and SiO_2 alignment both show a dark field in Fig. 5(b) and (c), respectively, which indicates better LC alignment in the prism area. Since it was suspected that direct rubbing on the prism may induce some damage, the defects in the liquid crystal texture as observed in Fig. 5(b) do not come as a surprise. For the SiO_2 alignment, based on obliquely evaporated SiO_2 layers, uniform darkness is observed in the prism area, implying that the LC molecules are perfectly aligned along the groove direction. With a high voltage $(100\ V_{pp})$ applied, most of the liquid crystal molecules are expected to be aligned parallel to the electric field (in the direction perpendicular to the glass substrates). In that situation, the polarization of the incident light is not changed and therefore blocked by the top analyzer, resulting in a uniform dark field as shown in Fig. 5(d)–(f).

From the above microscopic observations, we conclude that SiO_2 alignment, in which the alignment layers of the liquid crystal are produced by oblique evaporation of SiO_2, achieves the best LC alignment along the prism grooves. However, there are still some noticeable bright lines in the liquid crystal textures with and without electric field, as well as in single sided nylon alignment and hybrid rubbing alignment. Since these bright lines do not show up when we look at the bare prism in air between crossed polarizers, we can rule out diffraction or scattering as a possible cause. Instead, we believe they are due to imperfections in the liquid crystal alignment in the immediate vicinity of the tips and edges of the micro-prism structures, resulting in part of the incoming linearly polarized light being converted to elliptically polarized light.

3.3. Optical Measurement for Active Beam Steering Components

The optical setup that was used for characterizing the active LC components is schematically illustrated in Fig. 6. A He-Ne laser with $\lambda = 543$ nm is normally incident on the sample, and the transmission axis of the polarizer is parallel to the LC alignment within the active prism. The diffraction pattern is projected onto a semi-transparent screen and captured by an imaging camera behind the screen. Since the operating voltage is high due to the thick prism structure (8.5 μm in thickness) between the two ITO electrodes, the voltage signal from an arbitrary waveform generator (Agilent 33220A) is first amplified with a factor 10 by a high voltage linear amplifier (F10AD, FLC Electronics AB) and then applied to the active LC device.

The imaging camera (Nikon 1 J2) delivers raw sensor data from which we can derive the intensity of each diffraction order peak. This will allow us to determine the resultant steering angle of the switchable LC active prisms. In order to avoid clipping of the measured intensities, the camera settings (exposure time and diaphragm) are chosen such that nowhere inside the picture area saturation occurs. The image processing is as follows: first, the proprietary Nikon. NEF files are transformed into .DNG files using the Adobe DNG (Digital Negative) Converter. Next we import the DNG file into MATLAB. The image is then cropped so that only the area of the (horizontally oriented) diffraction pattern remains. Next, the horizontal center line of the diffraction pattern is considered and the measured intensity is plotted versus the index (location)

of the pixels. To accurately determine the intensity in every horizontal position, we use the value that results from integrating the intensity of all the individual pixels in each (vertical) column of the diffraction pattern. Subsequently, we apply a low pass filter along the horizontal axis to further reduce the noise. Equations (1) and (2), are used to assign suitable indices (N_{index}) to the pixels on the two sides of the original beam spot position (i.e., the zeroth order):

$$N_{low} = -\frac{L_-}{L_- + L_+} \times N \tag{1}$$

$$N_{high} = \left(1 - \frac{L_-}{L_- + L_+}\right) \times N \tag{2}$$

where L_- is the length measured from the original beam spot position to the right edge in the picture; L_+ is the length measured from the original beam spot position to the left edge; N is the total pixel number of the slice image in width (1952 pixels); N_{low} and N_{high} are new pixels indices for the two pixels on the right and left edges of the picture, respectively, and the rest of the pixels are between N_{low} and N_{high}. To derive the plot of the intensity versus angles instead of pixel indices, from the optical setup in Fig. 6, an equation is obtained:

$$\theta = \arctan\frac{N_i \times L}{N \times Y} \tag{3}$$

where Y is the distance between the sample and the screen, L is the total length of the diffraction pattern in the picture and equals $L_- + L_+$, and N_i is the index of a pixel from the new index array N_{index}. Since the diffraction angle of each order is discrete, by changing the relative refractive index difference between liquid crystal and micro-prism, the steering angle of the device could be shifted to either one of the diffraction orders or in between two diffraction orders. A simple linear interpolation is applied to the two peaks with the maximum intensity and second maximum intensity to derive a first order approximation of the beam steering angle of the active LC prism:

$$\theta_{steering} = \frac{\theta_{max} \times I_{max} + \theta_{submax} \times I_{submax}}{I_{max} + I_{submax}} \tag{4}$$

where θ_{max} and I_{max} are the angle and intensity of the maximum peak, and θ_{submax} and I_{submax} are the angle and intensity of the second maximum peak, respectively. The steering angle $\theta_{steering}$ can thus be obtained for the active LC components as a function of applied voltage.

4. Result and Discussion

For the active LC components based on single sided nylon alignment, with or without a high electric field, there is no obvious difference in the diffraction patterns, which means that the samples of single sided nylon alignment cannot deflect the light beam. This is due to the poor LC alignment observed in Fig. 5(a). In this section, we mainly focus on the electro-optical characterizations of samples made with hybrid rubbing alignment and SiO_2 alignment.

4.1. Electro-Optical Performance With Laser Beam

The active LC component is placed in the optical set-up described in Fig. 6. Square waveforms $(f = 1\ kHz)$ with different amplitudes are applied to the two ITO electrodes. The steering performances of hybrid rubbing alignment and SiO_2 alignment are demonstrated in Fig. 7. It is clear that diffraction occurs when the laser beam impinges on the LC component. As the pitch of the micro-prism is rather small (50 μm), when using highly coherent laser light, diffraction is inevitable in the beam steering patterns.

The intensity of the brightest spot and the adjacent diffraction orders are respectively measured by an optical power meter with removal of the screen, for both of the two components with and without electric field, from which their corresponding diffraction efficiency can be derived (Tables 2 and 3). Without applying any voltage, two brighter spots are observed in

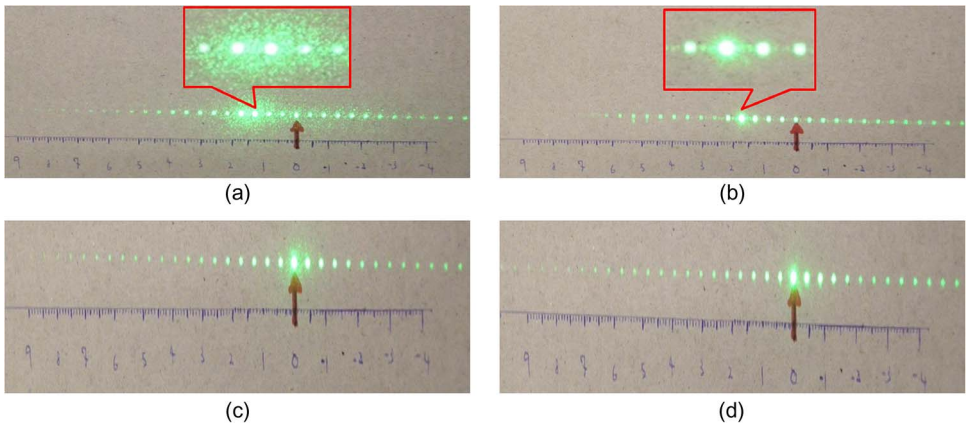

Fig. 7. Laser beam steering by active LC components. (a) Diffraction pattern of hybrid rubbing alignment without electric field. (b) Diffraction pattern of SiO_2 alignment without electric field. (c) Diffraction pattern of hybrid rubbing alignment with 100 V_{pp}. (c) Diffraction pattern of SiO_2 alignment with 100 V_{pp} (the red arrow indicates the original beam spot position, i.e., the zeroth order).

TABLE 2

Diffraction efficiency of hybrid rubbing alignment and SiO_2 alignment without applied voltage

Diffraction order	Efficiency of hybrid rubbing alignment (%)	Efficiency of SiO_2 alignment (%)
$+2_{nd}$	3.9	1.7
$+3_{rd}$	24.9	5.5
$+4_{th}$	19.8	41.6
$+5_{th}$	2.3	3.3

TABLE 3

Diffraction efficiency of hybrid rubbing alignment and SiO_2 alignment with 100 V_{pp}

Diffraction order	Efficiency of hybrid rubbing alignment (%)	Efficiency of SiO_2 alignment (%)
-2_{nd}	2.1	3.3
-1_{st}	9.2	10.2
0_{th}	65.7	58.4
$+1_{st}$	3.0	1.6
$+2_{nd}$	1.5	0.7

hybrid rubbing alignment with corresponding efficiency of 19.8% at the 4th order and 24.9% at the 3rd order, therefore we conclude that the peak of the diffraction envelope falls somewhere between the 3rd and the 4th order. In SiO_2 alignment, the peak falls more or less at the fourth order, showing one clear bright spot with a diffraction efficiency of 41.6%. In Fig. 7(a), it is observed that a lot of speckles appear around the diffraction pattern in hybrid rubbing alignment [magnified zone in the inlet of Fig. 7(a)], while SiO_2 alignment exhibits a very clear diffraction pattern. This could be explained by defects in the LC texture, caused by the rubbing process [see Fig. 5(b)], that strongly scatter the incident beam. These texture defects may further cause a different intensity distribution in the diffraction patterns between the two schemes. SiO_2 alignment with a higher uniformity of the LC alignment results in a higher equivalent refractive index (in the case of a positive uniaxial liquid crystal), and thus, gives a larger refractive index difference between the micro-prism and the liquid crystal layer, leading to a shift of the diffraction envelope to a larger steering angle. With a high voltage of 100 V_{pp}, both hybrid rubbing alignment

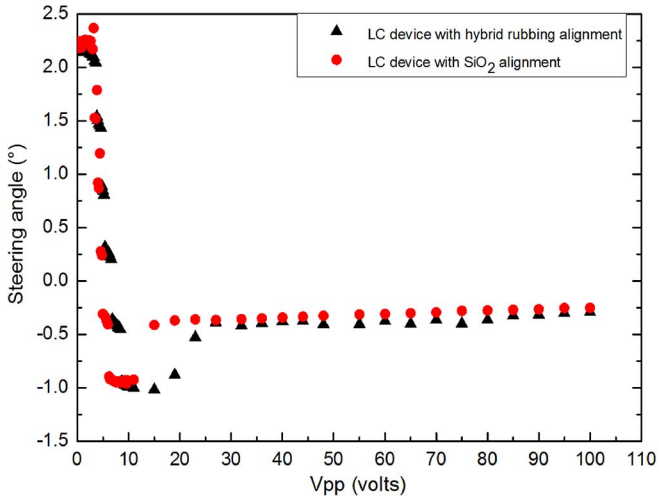

Fig. 8. Steering angle versus applied voltage for active LC beam steering components based on hybrid rubbing alignment (black triangles) and SiO_2 alignment (red circles).

and SiO_2 alignment shift the maximum intensity to the 0th order with a diffraction efficiency of 65.7% and 58.4%, respectively. Furthermore, the diffraction patterns look very similar.

With the methods mentioned in Section 3.3, the exact steering angles of the two active LC components with different applied voltages are derived from the original raw image files (Nikon. NEF files) using MATLAB, and the results are plotted in Fig. 8. It is seen that there is a threshold voltage in both hybrid rubbing alignment $(V_{th} = 2.4\ V_{pp})$ and SiO_2 alignment $(V_{th} = 2.6\ V_{pp})$, while the maximum steering angles with applied voltages below the thresholds are respectively 2.2° and 2.3° for both aligning schemes. Referring to Fig. 2, the NOA 74 prism has a refractive index of 1.52 which closely approximates the ordinary refractive index $(n_o = 1.5224)$ of the E7 liquid crystal. When the polarization of the incident laser beam is parallel to the direction of the liquid crystal alignment, the linearly polarized light meets the extraordinary refractive index $(n_e = 1.7394)$ of E7 which is larger than that of the NOA 74 UV prism. In that case it undergoes a deflection at the LC-prism surface and the beam spot is steered to a higher diffraction order [see Fig. 7(a) and (b)]. The deflection here satisfies Snell's law, using which the refraction angle is calculated to be 1.5°. Also taking the refraction occurring at the glass-air surface of the bottom glass substrate into account, we get the final deflecting angle of 2.3°, which is very close to the measured values in both schemes.

With increasing voltage, the steering angles start to decrease, and gradually move into the opposite side (the right side of the original beam spot position) for both schemes, and the lowest steering angle reached is about −1°. There is a range of 3° for the beam steering manipulations in the two components, and the corresponding operation voltage is below 10 V_{pp}, which is of great advantage for various optoelectronic applications. When the applied voltage is further increased above 20 V_{pp}, the steering angles are not obviously changed any more, which means both components enter into a saturation state. With a high voltage of 100 V_{pp}, the steering angles are still not zero, but there is a maximum intensity at the zeroth order, and other diffraction orders are still visible on the screen, as shown in Fig. 7(c) and (d). Even with a very strong electric field, most of the LC molecules realign parallel to the electric field, but there is still a small fraction of all LC molecules orienting toward the initial state which is along the prism groove due to the surface anchoring effect. Moreover, due to the designed prism profile, the thickness of the micro-prism is not uniform in the cross-section. The electric field distribution at the prism tips/edges is different from that in the middle of the LC layer, some LC molecules follow the non-uniformly distributed local electric field. Because of aforementioned two effects, polarized light experiences a small periodic refractive index difference at the

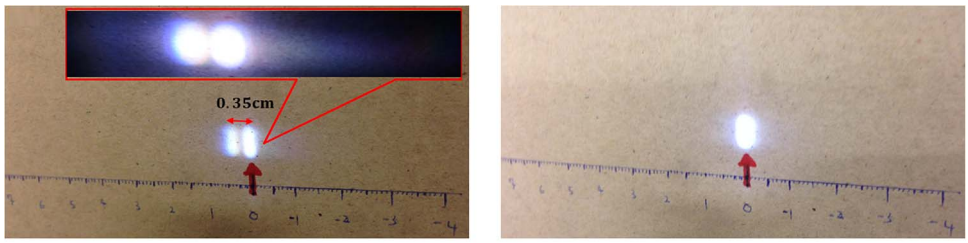

(a) (b)

Fig. 9. White light beam steering performance of hybrid rubbing alignment at (a) V = 0 V_{pp} and (b) V = 100 V_{pp}.

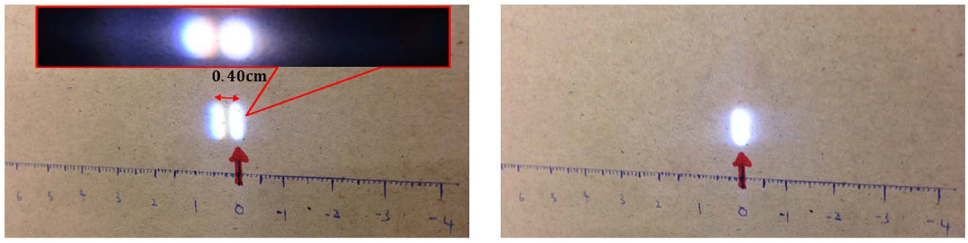

(a) (b)

Fig. 10. White light beam steering performance of SiO_2 alignment at (a) V = 0 V_{pp} and (b) V = 100 V_{pp}.

LC-prism boundaries, hence, diffraction persists for both hybrid rubbing alignment and SiO_2 alignment even with 100 V_{pp}.

4.2. Electro-Optical Performance With Collimated White Light

The LC beam steering components are also characterized using collimated white light. The optical setup is very similar to the one shown in Fig. 6, in which the laser is replaced by a white light source and two convex lenses. The function of the two lenses is to produce a collimated white light beam with a small spot size.

The white light beam steering performance of hybrid rubbing alignment and SiO_2 alignment is respectively demonstrated in Figs. 9 and 10. Since there is no polarizer used in the measurements, without applying the voltage, when the unpolarized and collimated white light passes through the liquid crystal layer within the component, it is divided into two rays: the ordinary ray and extraordinary ray, which separately undergo two different refractive indices n_o and n_e. Recall that the ordinary refractive index is equal to that of the UV prism, and their magnitudes are both smaller than the extraordinary one. The ordinary ray passes through the device, there is no refractive index difference between the LC layer and the UV prism, so it is not deflected and normally incident on the original spot position. For the extraordinary ray, which undergoes different refractive indices at the LC-prism surface, it is deflected away from the ordinary beam spot [Figs. 9(a) and 10(a)]. And the deflecting angles of the extraordinary rays in the two schemes are both measured: hybrid rubbing alignment achieves a steering angle of 1.9° with steering efficiency of 27.4%. For SiO_2 alignment, it has a steering angle of 2.2° with steering efficiency of 32.5%. These steering angles are close to those obtained with the laser beam and the calculated results using Snell's law. With a voltage of 100 V_{pp}, the liquid crystal molecules realign parallel to the electric field, the unpolarized white beam is not separated into two rays anymore, and the refractive indices are the same for the LC layer and the UV prism. Therefore, the light is not deflected and there is only one spot at the original spot position [see Figs. 9(b) and 10(b)].

It is noticed that there exist some “rainbows” at the two sides of the bright spots in both of the two schemes [shown in the inlets of Figs. 9(a) and 10(a) captured in a darker background],

which are also observed in the deflecting pattern of the bare UV prism. This is because the diffraction itself is dependent on the wavelength. In addition, both the liquid crystal and UV prisms are dispersive in the visible range, so the refraction occurring at the LC-prism surface is also dependent on the wavelength. Both factors contribute to the dispersion in the beam steering performance of the LC components. By optimizing the liquid crystals and UV resins with low dispersion, the dispersive phenomenon could be further reduced.

5. Conclusion

In this work, we successfully fabricated polymer micro prisms using soft embossing with elastic PDMS molds and different UV curable resins. The dimensions of the replicated prisms closely approximate those of the master prism, and both the PDMS mold and the UV replicas show better surface roughness than that of the master mold. With two different schemes for the LC alignment, namely hybrid rubbing alignment and obliquely evaporated SiO_2 alignment, the LC molecules are well aligned along the prism groove direction in both cases, although there are some defects in the LC textures of hybrid rubbing alignment. The operation voltage is relatively low (20 V_{pp}). In the on state, most of the laser beam energy is shifted back to the original beam spot position, but the diffraction orders still exist. Without applying voltages, the LC components shift the maximum intensity of the laser beam to other higher orders due to the refractive index difference at the LC-prism boundary. The graphs of the steering angle versus the applied voltage reveal a maximum steering angle of about 2°, and the total steering range is 3°. The LC active devices also demonstrate good steering performance with collimated white light, and the beam steering results are compatible with those with the laser beam and the theoretical calculations based on Snell's law. This effective beam steering component with optimized design and material choice will be of great benefit to the newly emerging applications (stage lighting, laser optics, and autostereoscopic displays).

Acknowledgment

The authors thank the Hercules foundation for providing funding for the APPLIE4MOS polymer prototyping line used in this research and Dr. ir. J. Missinne for his help with PDMS processing.

References

[1] F. M. Tapos *et al.*, "High bandwidth fast steering mirror," *Proc. SPIE*, vol. 5877, 2005, Art. ID. 587707.
[2] C. Schwarze, "A new look at Risley prisms." [Online]. Available: http://www.photonics.com/Article.aspx?AID=25652
[3] Y. Tajima and Y. Yamada, "Design of shaped dielectric lens antenna for wide angle beam steering," *Electron. Commun. Jpn.*, vol. 89, no. 2, pp. 1–12, Aug. 2006.
[4] A. Tuantranont *et al.*, "Optical beam steering using MEMS-controllable microlens array," *Sens. Actuators A, Phys.*, vol. 91, no. 3, pp. 363–372, Jul. 2001.
[5] T. K. Chan *et al.*, "Optical beamsteering using an 8 × 8 MEMS phased array with closed-loop interferometric phase control," *Opt. Exp.*, vol. 21, no. 3, pp. 2807–2815, Feb. 2013.
[6] Y. Sabry, D. Khalil, B. Saadany, and T. Bourouina, "Wide steering angle microscanner based on curved surface," *Proc. SPIE*, vol. 8616, Mar. 2013, Art. ID. 86160F.
[7] T. Scharf, *Polarized Light in Liquid Crystal and Polymers*. Hoboken, NJ, USA: Wiley, pp. 121–139, 2007.
[8] D. K. Yang and S. T. Wu, *Fundamentals of Liquid Crystal Devices*. Hoboken, NJ, USA: Wiley, pp. 107–155, 2006.
[9] Y. C. Chang, T. H. Jen, C. H. Ting, and Y. P. Huang, "High-resistance liquid-crystal lens array for rotatable 2D/3D autostereoscopic display," *Opt. Exp.*, vol. 22, no. 3, pp. 2714–2724, Feb. 2014.
[10] Q. S. Liao, C. M. Yang, C. W. Chen, and C. C. Hsiao, "A novel electrode structure of LCL lens designed for 55-in. 3D/2D switchable auto-stereoscopic display," in *Proc. IDW*, 2013, pp. 1041–1044.
[11] M. Kawamura, K. Nakamura, and S. Sato, "Liquid-crystal micro-lens array with two-divided and tetragonally hole-patterned electrodes," *Opt. Exp.*, vol. 21, no. 22, pp. 26 520–26 526, Nov. 2013.
[12] H. Ren, S. Xu, and S. T. Wu, "Polymer-stabilized liquid crystal microlens array with large dynamic range and fast response time," *Opt. Lett.*, vol. 38, no. 16, pp. 3144–3147, Aug. 2013.
[13] S. Valyukh, V. Chigrinov, H. S. Kwok, and H. Arwin, "On liquid crystal diffractive optical elements utilizing inhomogeneous alignment," *Opt. Exp.*, vol. 20, no. 14, pp. 15 209–15 221, Jul. 2012.
[14] C. J. Hsu and C. R. Sheu, "Preventing occurrence of disclination lines in liquid crystal lenses with a large aperture by means of polymer stabilization," *Opt. Exp.*, vol. 19, no. 16, pp. 14 999–15 008, Aug. 2011.
[15] S. Y. Chou, P. R. Krauss, and P. J. Renstrom, "Imprint of sub-25 nm vias and trenches in polymers," *Appl. Phys. Lett.*, vol. 67, no. 21, pp. 3114–3116, Nov. 1995.

[16] J. Kim *et al*., "Formation of the overcoat layer and column spacer for TFT-LCD using capillary force lithography," *Displays*, vol. 31, no. 2, pp. 82–86, Apr. 2010.
[17] S. Takei and A. Sekiguchi, "Nanoimprint resist material containing ultraviolet reactive fluorine surfactant for defect reduction in lithographic fabrication," *Appl. Sci.*, vol. 2, no. 1, pp. 24–34, Jan. 2012.
[18] H. B. Jo, K. J. Byeon, H. Lee, M. H. Kwon, and K. W. Choi, "Fabrication of ZnO nano-structures using UV nanoimprint lithography of a ZnO nano-particle dispersion resin," *J. Mater. Chem.*, vol. 22, pp. 20 742–20 746, 2012.
[19] S. H. Park, W. I. Lee, S. N. Moon, Y. E. Yoo, and Y. H. Cho, "Injection molding micro patterns with high aspect ratio using a polymeric flexible stamper," *Exp. Polym. Lett.*, vol. 5, no. 11, pp. 950–958, 2011.
[20] V. Mishra, G. S. Khan, K. D. Chattopadhyay, K. Nand, and R. G. V. Sarepaka, "Effects of tool overhang on selection of machining parameters and surface finish during diamond turning," *Measurement*, vol. 55, pp. 353–361, 2014.
[21] D. Yun *et al*., "Development of roll-to-roll hot embossing system with induction heater for micro fabrication," *Rev. Sci. Instrum.*, vol. 83, no. 1, Jan. 2012, Art. ID. 015108.
[22] I. Savu, S. Savu, and N. Sirbu, "Heat affected zones in polymer laser marking," *J. Thermal Anal. Calorimetry*, vol. 115, no. 2, pp. 1427–1437, Feb. 2014.
[23] *UV/EB Brochure*, RadTech Europe. [Online]. Available: http://www.radtech-europe.com
[24] *NOA Optical Adhesives*, Norland Products Inc. [Online]. Available: https://www.norlandprod.com
[25] K. J. Sohn, J. H. Park, D. E. Lee, H. I. Jang, and W. I. Lee, "Effects of the process temperature and rolling speed on the thermal roll-to-roll imprint lithography of flexible polycarbonate film," *J. Micromech. Microeng.*, vol. 23, no. 3, 2013, Art. ID. 035024.
[26] J. John, Y. Tang, J. P. Rothstein, J. J. Watkins, and K. R. Carter, "Large-area, continuous roll-to-roll nanoimprinting with PFPE composite molds," *Nanotechnology*, vol. 24, no. 50, Dec. 2013, Art. ID. 505307.
[27] D. Andrienko *et al*., "Electrically controlled director slippage over a photosensitive aligning surface in-plane sliding mode," *Liquid Crystals*, vol. 27, no. 3, pp. 365–370, 2000.
[28] X. Nie, R. Lu, H. Xianyu, T. X. Wu, and S. T. Wu, "Anchoring energy and cell gap effects on liquid crystal response time," *J. Appl. Phys.*, vol. 101, no. 10, May 2007, Art. ID. 103110.
[29] K. Takatoh *et al*., *Alignment Technologies and Applications of Liquid Crystal Devices*. New York, NY, USA: Taylor & Francis, pp. 7–98, 2005.